

Soft fundamental measure theory functional for the Weeks-Chandler-Andersen repulsive potential

K. L. Finster , Eric J. Krebs , Christopher J. May , Patrick A. Kreitzberg , and David Roundy 
Department of Physics, Oregon State University, Corvallis, Oregon 97331, USA

 (Received 30 September 2022; accepted 2 December 2022; published 27 December 2022)

We introduce a soft fundamental measure theory functional for the purely repulsive Weeks-Chandler-Andersen (WCA) fluid. This classical density functional could serve as a reference fluid for functionals created using thermodynamic perturbation theory instead of the hard-sphere fluid. Our functional incorporates temperature-dependent parameters describing the length scale and effective softness of the particle interaction, and which reproduce the second virial coefficient of the WCA fluid. We find that this approach is comparable in accuracy to the Barker-Henderson approach combined with the White Bear density functional for the hard-sphere fluid.

DOI: [10.1103/PhysRevE.106.064134](https://doi.org/10.1103/PhysRevE.106.064134)

I. INTRODUCTION

The idea of liquids as composed of hard spheres dates back over two millennia [1]. A hard-sphere fluid is characterized by a repulsive interatomic potential that goes instantly to infinity when two spheres come into contact. In the 20th century, it came to be understood that atoms are inherently soft with no abrupt border, but that their repulsion could still be accurately described using a hard-sphere fluid provided the diameter is chosen to be temperature dependent [2–4]. A temperature-dependent hard-sphere diameter reflects the effect of collisions during which the centers of two spheres come closer together at higher temperatures.

A hard-sphere fluid can be used as a reference fluid to which an attractive potential can be added as a perturbation [5]. A more realistic reference fluid would have a soft, repulsive interatomic potential like that of the Lennard-Jones potential between two neutral atoms. In the widely used Barker-Henderson (BH) approach, an arbitrary soft, repulsive potential can be constructed by mapping it at each temperature to the potential exhibited between hard spheres with a diameter appropriately sized for each temperature [3]. Weeks, Chandler, and Andersen (WCA) constructed a soft-sphere reference fluid by separating the Lennard-Jones potential in such a way as to recreate the soft, repulsive potential that reproduces the repulsive force of a Lennard-Jones interaction [6]. The soft, repulsive WCA potential is given by

$$V_{\text{WCA}}(r) = \begin{cases} 4\epsilon\left[\left(\frac{\sigma}{r}\right)^{12} - \left(\frac{\sigma}{r}\right)^6\right] + \epsilon, & 0 < r < 2R \\ 0, & \text{otherwise,} \end{cases} \quad (1)$$

where ϵ and σ are the usual Lennard-Jones parameters and R is a single sphere radius which is related by $\sigma = 2^{5/6}R$.

The BH approach (where the hard-sphere diameter is dependent on temperature only) lends itself for use with fundamental measure theory [7,8] (FMT) from which the thermodynamic properties of the fluid can be found. FMT is a powerful classical density functional theory (DFT) developed by Rosenfeld for the hard-sphere fluid. Tarazona improved on

the functional by introducing a tensor weight [9] to eliminate the divergences that arise in highly inhomogeneous situations like freezing. Due to its combination of computational efficiency with accuracy, FMT has been used as the basis for a wide variety of classical density functionals [10–15].

The hard-sphere fluid is well understood and has served as the reference system of choice for the theory of liquids [16–19] not only for the homogeneous fluid [20] but also in the more challenging case of the inhomogeneous fluid [21–24]. However, the hard-sphere fluid remains a non-physical model, which can also be numerically inconvenient due to its discontinuous potential and the requirement for delta functions in computing weighted densities.

Working toward a more realistic model for liquids which deals only with smoothly varying potentials, Schmidt developed soft fundamental measure theory (SFMT) [25,26], which is a classical DFT that *directly* treats model fluids with soft, repulsive potentials in a framework based on the highly successful FMT developed for hard spheres. As in FMT, SFMT uses a set of weighted densities to express the free energy of the system as a functional of the number density $n(\mathbf{r})$. Schmidt's SFMT functional is constructed so as to yield results consistent with the low-density limit of the virial expansion and the limiting case of a zero-dimensional cavity which are known exactly. SFMT has been used to describe the behavior of a star polymer in solution [27–30], as well as repulsive potentials applicable to atoms [26,30]. In his 2010 review of FMT, Roth points out that the most important future developments in classical equilibrium DFT will involve treating soft repulsions and attractions [31].

In this paper, we introduce a functional for a classical *soft*-sphere fluid based on SFMT that incorporates temperature-dependent parameters which we use to recreate the soft, repulsive potential of a WCA fluid. Since the WCA potential reproduces the repulsive force of a Lennard-Jones interaction, it is an ideal model for interatomic repulsion. Our results, and those generated for the WCA fluid using the hard-sphere BH approximation, are compared to Monte Carlo (MC) simulations.

II. METHODS

A. Soft fundamental measure theory

As in FMT, the excess Helmholtz free energy of Schmidt's SFMT (designed for soft spheres) is a functional of the number density $n(\mathbf{r})$ written as an integral of free energy densities $\Phi_i(\mathbf{r})$,

$$F_{ex}[n(\mathbf{r})] = k_B T \int (\Phi_1(\mathbf{r}) + \Phi_2(\mathbf{r}) + \Phi_3(\mathbf{r})) d\mathbf{r}, \quad (2)$$

which are functions of a set weighted densities $\{n_i\}$:

$$\Phi_1 = -n_0 \ln(1 - n_3), \quad (3)$$

$$\Phi_2 = \frac{n_1 n_2 - \mathbf{n}_{V1} \cdot \mathbf{n}_{V2}}{1 - n_3}, \quad (4)$$

$$\Phi_3 = \frac{1}{24\pi(1 - n_3)^2} \left(n_2^3 - 3n_2 \mathbf{n}_{V2} \cdot \mathbf{n}_{V2} + \frac{9}{2} [\mathbf{n}_{V2} \cdot \overleftrightarrow{\mathbf{n}}_{m2} \cdot \mathbf{n}_{V2} - \text{Tr}(\overleftrightarrow{\mathbf{n}}_{m2}^3)] \right). \quad (5)$$

Here we have used the tensor version of Φ_3 formulated by Tarazona [9,32] to give improved results for the crystallization of hard spheres. The weighted densities are given by

$$n_i(\mathbf{r}) = \int n(\mathbf{r}') w_i(|\mathbf{r} - \mathbf{r}'|) d\mathbf{r}' \quad (6)$$

and are defined as convolutions with weight functions similar to those of Rosenfeld's hard-sphere FMT [7]. As in FMT, the SFMT weight functions are constructed so as to deconvolve the Mayer function,

$$f(r) = e^{-\beta V(r)} - 1, \quad (7)$$

where $\beta = 1/k_B T$. The SFMT weight functions differ from those of FMT, however, and are given by

$$w_1 = \frac{w_2}{4\pi r}, \quad w_0 = \frac{w_2}{4\pi r^2}, \quad (8)$$

$$\mathbf{w}_{V2} = w_2 \frac{\mathbf{r}}{r}, \quad \mathbf{w}_{V1} = w_1 \frac{\mathbf{r}}{r}, \quad (9)$$

$$\overleftrightarrow{w}_{m2} = w_2(r) \left(\frac{\mathbf{r}\mathbf{r}}{r^2} - \frac{I}{3} \right), \quad (10)$$

$$w_3(r) = \int_r^\infty w_2(r') dr'. \quad (11)$$

Schmidt proved that as in traditional hard-sphere FMT, SFMT reproduces the exact functional in the low-density limit, provided the weight function w_2 that defines n_2 is related to the slope of the Mayer function by a convolution with itself:

$$\frac{df(r)}{dr} = \int_{-\infty}^\infty dr' w_2(r') w_2(r - r'). \quad (12)$$

By finding a weight function $w_2(r)$ that satisfies Eq. (12), a complete set of weight functions can be constructed since they all relate to $w_2(r)$.

One way to satisfy Eq. (12) is to choose a pair potential $V(r)$ and deconvolve the Mayer function $f(r)$ to solve for $w_2(r)$. However, deconvolving the Mayer function for a realistic potential is challenging. In the original papers introducing SFMT, Schmidt exclusively studied models analytically in which the potential is proportional to temperature [25,26].

While this proportionality is correct for purely entropic interactions, such as the star polymer in solution studied in several papers [25], this assumption is not applicable to energetic interactions such as dominate the repulsion between molecules.

Another way to satisfy Eq. (12) is to construct a $w_2(r)$ and solve for the pair potential to which that weight function corresponds. This is the approach we use in this paper. We use a weight function for $w_2(r)$ which has a Gaussian form as introduced by Schmidt [26],

$$w_2(r) = \frac{\sqrt{2}}{\Xi\sqrt{\pi}} e^{-\left(\frac{r-\alpha/2}{\frac{\Xi}{\sqrt{2}}}\right)^2}, \quad (13)$$

where Ξ and α are parameters with dimensions of length. This model, called the *error function model* or *erf model*, results in analytically simple forms for the $w_3(r)$ weight function, the Mayer function, and the pair potential:

$$w_3(r) = \frac{1}{2} \left(1 - \text{erf} \left(\frac{r - \alpha/2}{\frac{\Xi}{\sqrt{2}}} \right) \right), \quad (14)$$

$$f(r) = \frac{1}{2} \left(\text{erf} \left(\frac{r - \alpha}{\Xi} \right) - 1 \right), \quad (15)$$

$$V_{\text{erf}}(r) = -k_B T \ln \left[\frac{1}{2} \left(\text{erf} \left(\frac{r - \alpha}{\Xi} \right) + 1 \right) \right]. \quad (16)$$

In the next section, we will modify the erf model to create a functional that can be used to model a soft-sphere fluid like the WCA fluid.

B. Soft FMT for the WCA fluid

As is evident from Eqs. (16) and (15), a potential energy of interaction that is temperature independent, like that of the WCA fluid, can only be modeled at one temperature using the error function model. At other temperatures, the Mayer function $f(r)$ for the WCA potential takes on an entirely different form than that produced by the erf potential and is not analytically tractable.

To use the erf potential to approximately reproduce the soft, repulsive, temperature-independent potential of the WCA fluid at each temperature, we offset the original temperature dependence of the erf potential by making the α and Ξ parameters temperature dependent. This is analogous to how Barker and Henderson introduced a temperature-dependent hard-sphere radius to use the entropically dominated hard-sphere fluid to approximate a soft, repulsive potential. The α parameter roughly measures the length scale of the interaction and decreases with increasing temperature like the BH diameter. The Ξ parameter is a measure of the effective softness of the interaction and increases with the temperature.

We obtain an expression for Ξ by considering that as the distance r between the centers of two spheres increases, the potential drops from infinity to zero, and the Mayer function changes from -1 to 0 . The wider the distance over which the Mayer function changes rapidly, the softer the potential and the greater the width of the curve of the derivative of the Mayer function plotted versus the distance r . Thus, we achieve comparable softness by matching the widths of the derivatives of the Mayer functions for the WCA and the erf potentials.

The derivative of the Mayer function for the erf potential is computed by putting $w_2(r)$, given by Eq. (13), into Eq. (12). This gives

$$\frac{df_{\text{erf}}(r)}{dr} = \frac{1}{\Xi\sqrt{\pi}} e^{-\left(\frac{r-\alpha}{\Xi}\right)^2}, \quad (17)$$

with a width, or variance, given by $\Xi/\sqrt{2}$. We then relate the parameter Ξ to the variance of the radius about the peak of the derivative of the Mayer function for the WCA potential $f'_{\text{WCA}}(r)$ computed at a given temperature,

$$\frac{\Xi^2}{2} = \langle r^2 \rangle - \langle r \rangle^2, \quad (18)$$

where

$$\langle r \rangle = \frac{\int f'_{\text{WCA}}(r) r dr}{\int f'_{\text{WCA}}(r) dr}. \quad (19)$$

To obtain an expression for α , we set the second virial coefficient B_2 of the WCA fluid computed using the WCA potential given in Eq. (1) equal to the second virial coefficient computed using the erf potential given in Eq. (16), and solve for the parameter α at a given temperature. The second virial coefficient is related to the Mayer function [which passes through $-1/2$ at $r = \alpha$ in Eq. (15)] and is sensitive to the length-scale of the interaction:

$$B_2 = -\frac{1}{2} \int f(r) d\mathbf{r} \quad (20)$$

$$= -\frac{1}{2} \int (e^{-\beta V(r)} - 1) d\mathbf{r}. \quad (21)$$

Matching the second virial coefficient to that of the WCA fluid makes the first-order correction to the pressure equal to that of a WCA fluid in the low-density limit, where it is not likely to find more than two particles in close proximity at any point in time.

$$\frac{P}{k_B T n} = 1 + nB_2 + \dots \quad (22)$$

The erf potential given in Eq. (16) with temperature-dependent parameters α and Ξ is plotted in Fig. 1 at three different temperatures alongside the WCA potential. The largest deviations are seen at very small distances, and thus very high potential energies. The derivative of the Mayer function corresponding to the WCA pair potential is shown in Fig. 2, where it is compared to w_2 given in Eq. (13) convolved with itself. Ideally, the curves would match for each temperature, provided Eq. (12) is satisfied.

C. Freezing of the WCA fluid

In classical DFT, the equilibrium density $n(\mathbf{r})$ is that which minimizes the Helmholtz free energy for a fixed number of particles N and volume V at a given temperature. Like the hard-sphere fluid, the WCA fluid freezes into the face-centered-cubic crystal structure. We represent $n(\mathbf{r})$ for this crystalline state as a sum of Gaussian functions, each centered

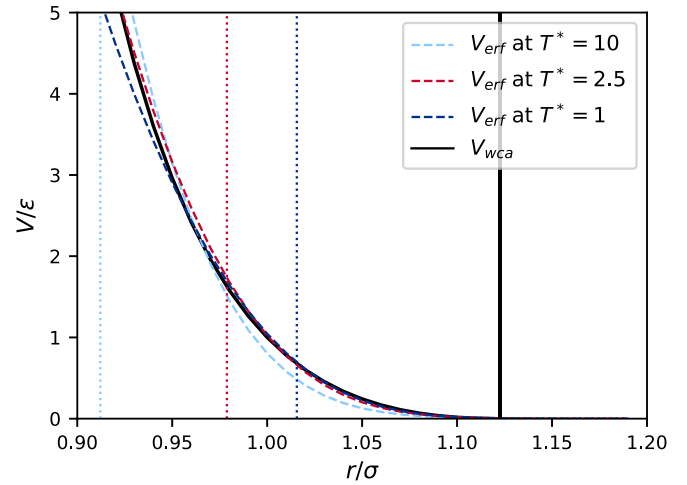


FIG. 1. The WCA potential (solid line curve) is shown along with approximations to this potential at three different reduced temperatures ($T^* = k_B T / \epsilon$) constructed using the erf potential (dashed lines) with incorporated temperature-dependent parameters α and Ξ . The vertical dotted lines show the values of α at which V_{erf} and V_{WCA} would ideally be matched, and the solid black vertical line represents the distance at which the WCA force goes to zero. (Deviations near the bottom of the curve increase with temperature.)

at a lattice point specified by \mathbf{R}_i :

$$n(\mathbf{r}) = (1 - f_v) \sum_i \frac{1}{(\sqrt{2\pi}\sigma_g)^3} e^{-\left(\frac{|\mathbf{r}-\mathbf{R}_i|}{\sqrt{2}\sigma_g}\right)^2}. \quad (23)$$

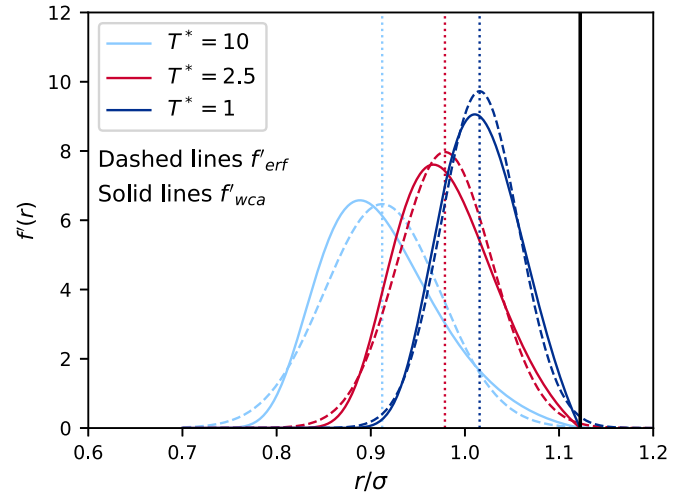


FIG. 2. The derivative of the Mayer function for the WCA potential f'_{WCA} (solid lines) and the convolution of w_2 with itself (which gives f'_{erf} plotted with dashed lines) are shown at three different temperatures. According to Eq. (12), these should be identical to accurately reproduce the low-density behavior of the fluid. The vertical dotted lines show values of α where the erf potential peaks, and the solid vertical line shows where the WCA force and f'_{WCA} go to zero. The erf result extends slightly past the cutoff at which f'_{WCA} vanishes for all temperatures, but goes quickly to zero. At lower temperatures, the curves become more peaked and approach the cutoff as the system approaches hard-sphere behavior at which they become Dirac delta functions.

The density can be varied spatially by changing the width of the Gaussians σ_g and the fraction of vacant lattice sites f_v while keeping the overall number density fixed. As the Gaussian width gets large, the number density becomes homogeneous, as would be expected for a fluid. Varying the fraction of vacancies while the overall number density is fixed changes the size of the crystal cell. A very small fraction of vacancies helps to avoid computational difficulties.

We use MC integration with importance sampling to compute the weighted densities used in the Helmholtz free energy, which is then minimized. The pressure can be found from a finite difference approximation of the slope of the Helmholtz free energy per atom with respect to volume per atom. The pressure at the phase transition can be obtained from the crossing point in a plot of the Gibbs free energy per atom against pressure.

D. Comparison to Barker-Henderson hard sphere

The results from our soft-sphere SFMT method introduced in this paper will be compared with those obtained using the BH approximation. In the BH approach [3], a soft-sphere fluid with a repulsive pair potential $V(r)$ is approximated by a hard-sphere fluid with a temperature-dependent diameter given by

$$d_{\text{BH}} = \int_0^\infty (1 - e^{-\beta V(r)}) dr. \quad (24)$$

The BH approach is based on hard spheres, and so it can be used in conjunction with a hard-sphere functional.

We use the White Bear [11] functional with the BH diameter to generate density and radial distributions of the inhomogeneous WCA fluid. The White Bear functional is a modified version of Rosenfeld's FMT functional for hard spheres which uses the same weight functions as FMT (which differ from those of SFMT) and that are all based on a Dirac delta function for w_2 given by

$$w_2(r) = \delta(R - r), \quad (25)$$

where R is the hard-sphere radius. The White Bear functional uses the same Φ_1 and Φ_2 as in FMT [also given by Eqs. (3) and (4)], but Φ_3 is replaced with

$$\Phi_3 = (n_2^3 - 3n_2 \mathbf{n}_{V2} \cdot \mathbf{n}_{V2}) \frac{n_3 + (1 - n_3)^2 \ln(1 - n_3)}{36\pi n_3^2 (1 - n_3)^2}, \quad (26)$$

which reduces to the Carnahan-Starling equation of state rather than scaled-particle theory for homogeneous hard-sphere systems.

III. RESULTS

In this section, the results of our SFMT method introduced in this paper will be compared to those produced by the BH approximation. We will also compare our results with MC simulations of the WCA fluid.

A. Soft spheres in bulk

We begin by examining the equation of state of the bulk fluid. Figure 3 shows the pressure as a function of volume for a wide range of temperatures. A gray region between the solid

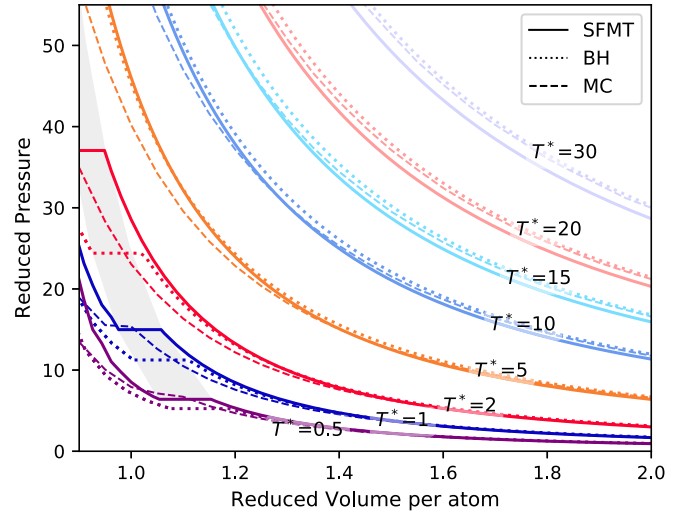


FIG. 3. Plot of the reduced pressure ($P\sigma^3/\epsilon$) versus the reduced volume per atom ($1/n\sigma^3$) for the WCA fluid. Solid lines give our SFMT results introduced in this work, and the gray region on the left indicates the coexistence region predicted by our SFMT method. Dashed lines show the results of our MC simulations (256 atoms). Dotted lines represent the BH approximation where the BH freezing and melting densities are derived using Eq. (24) together with hard-sphere packing fractions $\eta_f = 0.494$ and $\eta_m = 0.545$ [33]. BH fluid pressures are from the Carnahan-Starling equation of state, and BH crystal pressures are based on hard-sphere data from molecular dynamics simulations [33,34].

and fluid phases indicates the coexistence region as predicted by our SFMT method introduced in this paper. We find that at high volumes (low densities), both methods (this paper and BH) approach the correct MC pressures, as expected, although at higher temperatures, our SMFT method approaches the correct pressure more slowly than BH. As the volume decreases (density increases), both methods (this paper and BH) show increasingly higher pressures than the MC simulations when coming near the coexistence region. At freezing, the pressures predicted by our SMFT method are higher than those predicted by BH, and the difference between them increases with temperature. In the solid crystalline region, the results of our SMFT method exhibit higher pressures than the MC simulations, while BH follows the MC simulations more closely.

Figure 4 shows a phase diagram of the temperature versus the density for the WCA fluid. Again, a gray region between the fluid and solid phases indicates the coexistence region as predicted by our SFMT method introduced in this paper. We find that the freezing and melting densities predicted by our SMFT method show good agreement with MC simulations though shifted slightly to higher densities. The BH freezing and melting densities show lower values than the MC simulations and deviate increasingly as the temperature increases.

Overall, we found that our SFMT method introduced in this paper shows good agreement with MC simulations over a wide range of temperatures and densities, but predicts pressures that are too high for the solid crystal. The melting and freezing densities predicted by our SMFT method show much better agreement with MC simulations than BH.

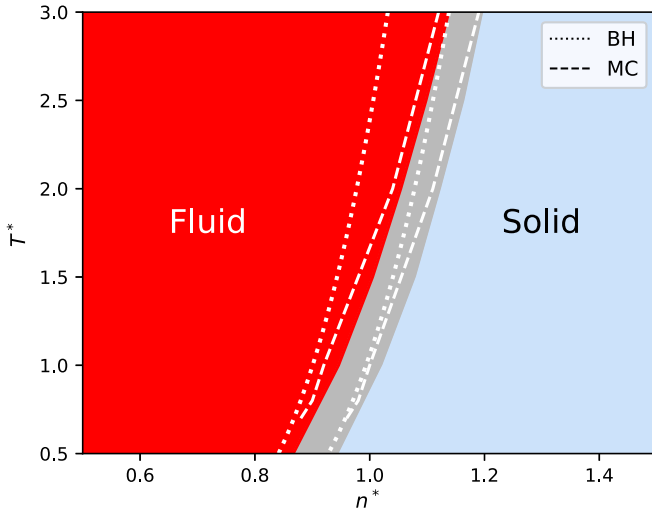


FIG. 4. Phase diagram of the reduced temperature versus the reduced density ($n^* = n\sigma^3$) for the WCA fluid. The narrow gray region between the fluid phase (on the left) and solid phase (on the right) is the region of coexistence generated using our SFMT method introduced in this paper. Dashed lines indicate freezing and melting densities from MC simulations [35] and dotted lines show BH freezing and melting densities derived using Eq. (24) together with hard-sphere packing fractions $\eta_f = 0.494$ and $\eta_m = 0.545$ [33].

B. Soft spheres near a hard wall

As the simplest test for inhomogeneous one-dimensional behavior, we plot density profiles for the WCA soft-sphere fluid near a hard wall. A hard wall, in this context, is interpreted as a potential encountered by the spheres that abruptly transitions from zero to infinity. Figure 5 shows density profiles for reduced densities of $n^* = 0.6$ and $n^* = 1.0$ at different temperatures.

We find that our SFMT method introduced in this paper and the BH approach with the White Bear hard-sphere functional give almost identical results. Both methods (this paper and BH) are in good agreement with the MC simulations overall with slight discrepancies in the position and height of the peaks, especially at the first peak, which increase with decreasing temperature or increasing density.

C. Soft spheres near a soft wall

As a second and more physical case, we construct a soft wall made of a continuum of soft WCA spheres with density ρ . The potential at a distance z from such a wall is given by

$$V_{\text{SW}}(0 < z \leq d) = 2\pi\rho\epsilon \left[\frac{2\sigma^{12}}{45} \left(\frac{1}{z^9} - \frac{1}{d^9} \right) + \frac{\sigma^6}{3} \left(\frac{1}{d^3} - \frac{1}{z^3} \right) + \frac{z^3 - d^3}{6} + (d - z) \left(\frac{d^2}{2} + \frac{\sigma^6}{d^4} - \frac{2\sigma^{12}}{5d^{10}} \right) \right], \quad (27)$$

where the distance $d = 2^{-5/6}\sigma$ is equal to the distance at which the interaction between WCA spheres vanishes. The Lennard-Jones parameters ϵ and σ in Eq. (27) are those between the wall and the fluid and are taken to be identical to

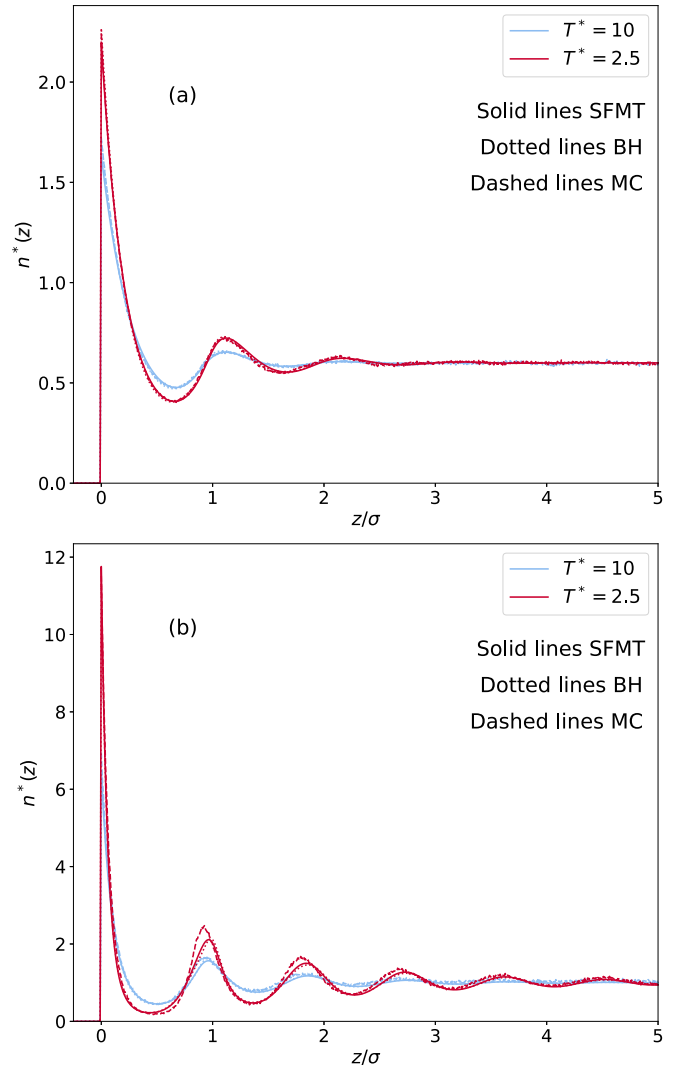


FIG. 5. Density distribution of the WCA fluid near a hard wall as a function of the reduced distance (z/σ) for reduced densities of (a) $n^* = 0.6$ and (b) $n^* = 1.0$. The solid lines give our SFMT results introduced in this paper, the dotted lines represent the BH approximation using the White Bear functional, and dashed lines give our MC simulation results. (Curves at lower temperatures show higher peaks.)

those within the fluid. The potential is zero when $z > d$, and is infinite for $z \leq 0$.

In Fig. 6, we plot the density versus the distance from the surface of the wall at different temperatures. Again, we find that our SFMT method introduced in this paper gives almost identical predictions to the BH approach, while both methods closely follow the MC simulations with slight discrepancies in the position and height of the peaks, especially at the first peak, which increase with decreasing temperature or increasing density.

D. Soft spheres radial distribution function

For three-dimensional comparisons, we plot radial distribution functions generated by using the Percus' test particle approach [36] in which a test sphere with a WCA potential

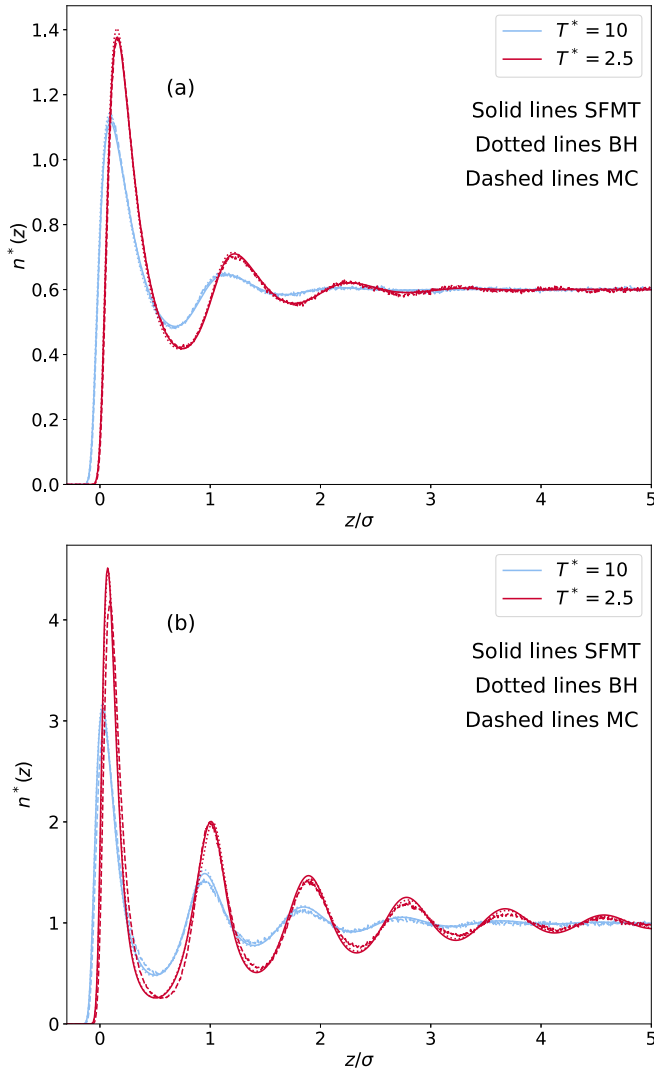


FIG. 6. Density distribution of the WCA fluid near a soft wall as a function of the reduced distance (z/σ) for reduced densities of (a) $n^* = 0.6$ and (b) $n^* = 1$. The solid lines give our SFMT results introduced in this paper, the dotted lines represent the BH approximation using the White Bear functional, and dashed lines give our MC simulation results. (Curves at lower temperatures show higher peaks.)

is surrounded by a WCA fluid. Figure 7 shows radial distribution functions at two different densities for a range of temperatures. We find that both our SFMT method introduced in this paper and the BH approximation are in almost exact agreement with the MC simulations with slight discrepancies in the position and height of the peaks, especially at the first peak, which increase with decreasing temperature or increasing density.

E. Argon

To make comparisons with experiment, we simulate the radial distribution function of argon under high pressure (which minimizes the effects of the attractive potential). We do this by computing the radial distribution of a WCA fluid surrounding a single Lennard-Jones test particle where we have used the

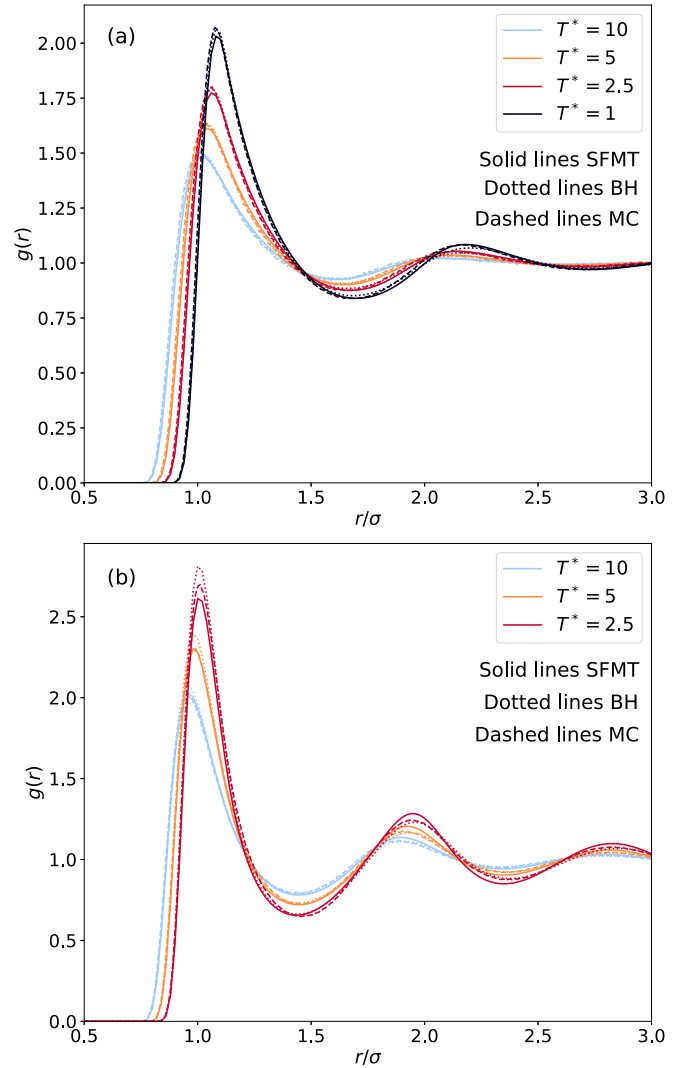


FIG. 7. Radial distribution function of the WCA fluid for reduced densities of (a) $n^* = 0.6$ and (b) $n^* = 1$. As in the other figures, the solid lines give our SFMT results introduced in this paper, the dotted lines represent the BH approximation using the White Bear functional, and dashed lines give our MC simulation results. (Curves at lower temperatures show higher peaks.)

Lennard-Jones parameters developed by Verlet: $\sigma = 3.405 \text{ \AA}$ and $\epsilon/k_B = 119.8 \text{ K}$ [37] for both our WCA fluid and the test particle. In Fig. 8, we show the results of three experiments for which data is available [38–40], and which roughly span the range of reduced densities from 0.6 to 1.0. The first experiment was performed at 148 K and 9.92 MPa, the second at 85K and vapor pressure, and the third at room temperature and 1.1 GPa. For each system, we compute the radial distribution function for argon using our SFMT method introduced in this paper, the BH approximation, and MC simulation.

From the results shown in Fig. 8, we note that our MC simulations of the WCA fluid give a reasonably good prediction of the radial distribution function of a real liquid, albeit with some discrepancies which increase with increasing density, especially at the first peak. We find that the results of our SFMT method introduced in this paper and those of the BH

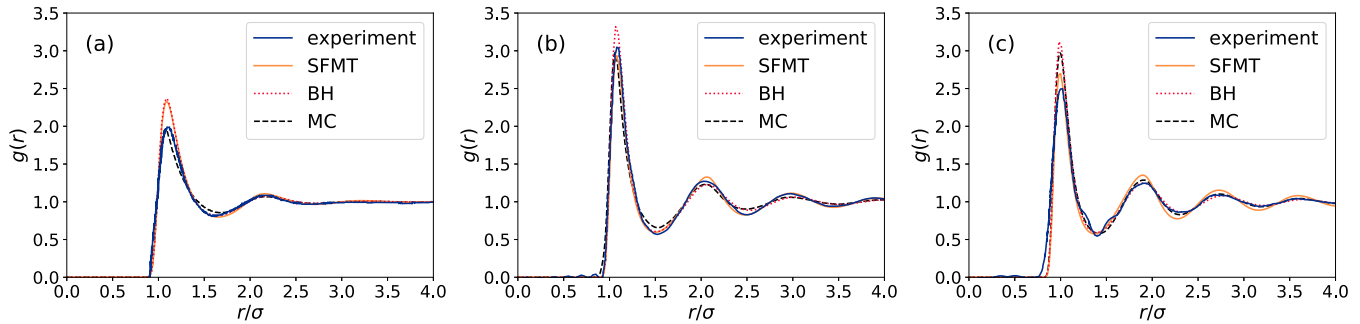


FIG. 8. Radial distribution functions of argon. The darker solid lines show the results of experiments, and the lighter solid lines show the results from simulations using our SFMT method introduced in this paper. The dotted lines show the results of the BH approximation using the White Bear functional and the dashed lines show the results of our MC simulations. (a) Experimental data taken at 148 K and 9.92 MPa, and simulated with $n^* = 0.5844$, $T^* = 1.235$. (b) Experimental data taken at 85 K and vapor pressure, and simulated with $n^* = 0.8389$, $T^* = 0.71$. (c) Experimental data taken at room temperature and 1.1 GPa, and simulated with $n^* = 1.0950$, $T^* = 2.48$.

approximation show good agreement overall with both the experimental results and MC simulations, with some slight discrepancies in the position and height of the peaks, especially at the first peak.

IV. CONCLUSION

We have developed a functional for a classical fluid with a soft, or smoothly varying, repulsive interatomic potential and applied it successfully to model the WCA soft-sphere fluid. Our functional is based on Schmidt's SMFT, designed to be applied directly to a soft-sphere fluid without the need to map a fluid with a soft potential to a hard-sphere fluid as is done in the widely used BH method. Similar to the BH method, which makes the hard-sphere radius temperature dependent, we also make parameters in our functional temperature dependent to characterize the length scale and softness of the particle interaction, and reproduce the second virial coefficient of the fluid.

In this paper, we demonstrated that our functional can be used to predict the equation of state and freezing and melting densities for the WCA fluid in good agreement with MC simulations over a wide range of temperatures and densities. We have also generated one-dimensional density profiles of the WCA fluid against hard and soft walls, and radial distribution functions which all show good agreement with MC simulations. We have also used our functional to simulate radial distribution functions of liquid argon that show good agreement with both MC simulations and experiments.

Overall, we found that our method presented in this paper is as good as the BH method over a wide range of densities and temperatures and at the freezing and melting densities, but not much further into the solid crystalline region. The advantage to our theory is that it is closer to modeling a real fluid which is naturally soft, and we can use it *as is* rather than needing to accommodate for discontinuities and delta functions of hard-sphere fluids.

-
- [1] Lucretius, *De rerum natura* (60 BCE).
- [2] J. S. Rowlinson, *Mol. Phys.* **8**, 107 (1964).
- [3] J. A. Barker and D. Henderson, *J. Chem. Phys.* **47**, 4714 (1967).
- [4] H. C. Andersen, J. D. Weeks, and D. Chandler, *Phys. Rev. A* **4**, 1597 (1971).
- [5] R. W. Zwanzig, *J. Chem. Phys.* **22**, 1420 (1954).
- [6] J. D. Weeks, D. Chandler, and H. C. Andersen, *J. Chem. Phys.* **54**, 5237 (1971).
- [7] Y. Rosenfeld, *Phys. Rev. Lett.* **63**, 980 (1989).
- [8] Y. Rosenfeld, M. Schmidt, H. Löwen, and P. Tarazona, *Phys. Rev. E* **55**, 4245 (1997).
- [9] P. Tarazona, *Phys. Rev. Lett.* **84**, 694 (2000).
- [10] J. A. Cuesta and Y. Martínez-Ratón, *Phys. Rev. Lett.* **78**, 3681 (1997).
- [11] R. Roth, R. Evans, A. Lang, and G. Kahl, *J. Phys.: Condens. Matter* **14**, 12063 (2002).
- [12] H. Hansen-Goos and K. Mecke, *Phys. Rev. Lett.* **102**, 018302 (2009).
- [13] M. Marechal and H. Löwen, *Phys. Rev. Lett.* **110**, 137801 (2013).
- [14] J. Hughes, E. J. Krebs, and D. Roundy, *J. Chem. Phys.* **138**, 024509 (2013).
- [15] E. J. Krebs, J. B. Schulte, and D. Roundy, *J. Chem. Phys.* **140**, 124507 (2014).
- [16] A. Gil-Villegas, A. Galindo, P. J. Whitehead, S. J. Mills, G. Jackson, and A. N. Burgess, *J. Chem. Phys.* **106**, 4168 (1997).
- [17] G. N. I. Clark, A. J. Haslam, A. Galindo, and G. Jackson, *Mol. Phys.* **104**, 3561 (2006).
- [18] T. Lafitte, A. Apostolakou, C. Avendaño, A. Galindo, C. S. Adjiman, E. A. Müller, and G. Jackson, *J. Chem. Phys.* **139**, 154504 (2013).
- [19] I. Nezbeda, M. Klajmon, and J. Hrubý, *J. Mol. Liq.* **362**, 119769 (2022).
- [20] N. F. Carnahan and K. E. Starling, *J. Chem. Phys.* **51**, 635 (1969).
- [21] G. Shen, Y. Sun, Y. Wang, X. Lu, and X. Ji, *J. Mol. Liq.* **310**, 113199 (2020).
- [22] V. M. Sermoud, G. D. Barbosa, E. do A. Soares, L. H. de Oliveira, M. V. Pereira, P. A. Arroyo, A. G. Barreto Jr., and F. W. Tavares, *Chem. Eng. Sci.* **247**, 116905 (2022).

- [23] G. Shen, D. Zhang, Y. Hu, X. Zhang, F. Zhou, Y. Qian, X. Lu, and X. Ji, *J. Chem. Phys.* **157**, 014701 (2022).
- [24] M. Bültmann and A. Härtel, *J. Phys.: Condens. Matter* **34**, 235101 (2022).
- [25] M. Schmidt, *Phys. Rev. E* **60**, R6291(R) (1999).
- [26] M. Schmidt, *Phys. Rev. E* **62**, 4976 (2000).
- [27] M. Schmidt, *Phys. Rev. E* **62**, 3799 (2000).
- [28] B. Groh and M. Schmidt, *J. Chem. Phys.* **114**, 5450 (2001).
- [29] S.-C. Kim, *J. Chem. Phys.* **114**, 9593 (2001).
- [30] M. B. Sweatman, *J. Phys.: Condens. Matter* **14**, 11921 (2002).
- [31] R. Roth, *J. Phys.: Condens. Matter* **22**, 063102 (2010).
- [32] A. Santos, *Phys. Rev. E* **86**, 040102(R) (2012).
- [33] W. G. Hoover and F. H. Ree, *J. Chem. Phys.* **49**, 3609 (1968).
- [34] A. R. Denton, N. W. Ashcroft, and W. A. Curtin, *Phys. Rev. E* **51**, 65 (1995).
- [35] C. May, *B.S. thesis, Oregon State University*, 2018.
- [36] J. K. Percus, *Phys. Rev. Lett.* **8**, 462 (1962).
- [37] L. Verlet, *Phys. Rev.* **159**, 98 (1967).
- [38] P. G. Mikolaj and C. J. Pings, *J. Chem. Phys.* **46**, 1401 (1967).
- [39] J. L. Yarnell, M. J. Katz, R. G. Wenzel, and S. H. Koenig, *Phys. Rev. A* **7**, 2130 (1973).
- [40] J. H. Eggert, G. Weck, P. Loubeyre, and M. Mezouar, *Phys. Rev. B* **65**, 174105 (2002).